A NOISE REDUCTION STUDY ON FLOW-PERMEABLE TRAILING-EDGES

M. Herr*

*Deutsches Zentrum für Luft- und Raumfahrt (DLR), Institute of Aerodynamics and Flow Technology
Lilienthalplatz 7, D-38108 Braunschweig, Germany

Key words: Aeroacoustics, Airfoil self-noise, Airframe noise, Trailing-edge noise reduction, Flow-permeable trailing-edges, Brushes, Edge condition, Trailing-edge combs, Edge modifications

Abstract: *This paper summarizes the results of an experimental study on flow-permeable comb-type trailing-edges which have the potential to effectively reduce turbulent boundary-layer trailing-edge noise. Basic design rules are presented with respect to a future use of such devices as suitable add-on solutions for a wide range of technical applications. These are e.g. the high-lift devices of current passenger aircraft, the blades of cooling fans or wind turbines which represent strong trailing-edge noise radiators. The noise reduction potential of several trailing-edge modifications, applied on a flat plate and on a two-dimensional NACA0012-like airfoil, was measured by a directional microphone in the open-jet anechoic Aeroacoustic Wind Tunnel Braunschweig. Additional knowledge of the incident boundary-layer flow properties was gained by application of hot-wire anemometry and unsteady surface pressure measurements. Within the range of parameters tested so far, comb design optimization appears mainly determined by geometric details of the comb itself than being dependent on specifics of the incident flow. Comb devices show the same (velocity)^5-scaling behaviour of farfield trailing-edge noise intensity as solid edges, however, on a significantly reduced level (-2 to -10 dB), and based on a constant scaling length. A minimum device length (in the order of the turbulent boundary-layer thickness δ_{99} or more) and a narrow slit width (of about the viscous sublayer thickness) were identified as the major design requirements. Flexibility of the comb material was found beneficial, but not essential to achieve a noise reduction.*

1. INTRODUCTION

As a claim of the European "Vision for 2020" [1] airframe noise levels of civil transport aircraft will have to be reduced by 10 dB per operation. In the final approach phase, at reduced thrust, relevant airframe noise contributors are the components of today's high-lift systems, such as the deployed slats or flaps. One of the prevalent noise mechanisms is trailing-edge (TE) scattering noise, i.e. an edge-enhanced conversion of turbulent energy (within the turbulent boundary-layer or shear-layer flow approaching the TE) into sound energy [2-4]. From Ffowcs-Williams and Hall [2] it is known that this process is directly related to the geometric discontinuity at the TE. On this basis it is concluded that edge modifications which provide a somehow "smoothed" TE boundary condition will reduce TE noise radiation efficiency. In search of applicable retrofit solutions for existing airframe components the principal noise reduction capability of flow-permeable edge-extensions (flexible "brushes" [5]) was proven in previous studies, e.g. [6]. A noteworthy example of their successful application at low *Re* numbers is given by some owl species, being almost inaudible for their prey, which make use of analogous noise reducing TE fringes at their primary feathers [7, 8].

The current work concentrates on the identification of the crucial design parameters and the corresponding TE noise scaling laws, which are needed for the transfer of such "owl technology" [8] to practical solutions. The discussion here confines to a more fundamental aeroacoustic viewpoint. To provide a systematic evaluation of single test parameters very simple two-dimensional reference airfoils were used, being far from most realistic applications with their complex three-dimensional flow fields. Therefore, the sensitive question whether the aerodynamic performance might be adversely affected by the noise reduction devices is not explicitly addressed at this stage of investigations. However, based on the findings of a recent CFD study on stiff comb-shaped modifications applied at a realistic A340-type slat TE [9], it is assumed that performance penalty can be avoided, if the comb devices are carefully integrated in the geometry.

2. EXPERIMENTAL SETUP

Experiments were conducted in the Aeroacoustic Wind Tunnel Braunschweig (AWB) of DLR, which is an open-jet closed-circuit anechoic test facility with a rectangular 0.8 m by 1.2 m nozzle exit. Two generic symmetrical airfoil configurations were used (Fig. 1); (i) a modular flat plate with variable chord length, ranging from 0.8 m to 2.0 m (*Re* = 2.1 Mio to 7.9 Mio), and (ii) a two-dimensional 0.4-m chord NACA0012-like airfoil (*Re* = 1.1 Mio to 1.6 Mio).

The 0.8-m span NACA0012-like airfoil was mounted horizontally between two vertical sidewalls at the AWB nozzle exit which allowed angle-of-attack variations. To provide validation against earlier published experimental TE noise data, chord-based *Re* numbers were comparable to those in extensive measurements by Brooks et al. [10, 11]. The airfoil, however, shows slight geometric differences when compared to the original NACA0012 coordinates, since the original NACA0012 TE thickness (h = 1.008 mm for a 0.4-m chord length) was reduced to h = 0.15 mm to provide a "sharp" solid reference TE [4]. The latter realized a thickness parameter of about $h/\delta^* = 0.07$, with δ^* being the boundary layer displacement thickness. This is clearly below the threshold of $h/\delta^* \approx 0.3$ for which blunt TE periodic vortex-shedding was found to vanish in previous NACA0012 experiments [11, 12]. As a consequence of these geometric changes (limited to the rear 20 % of the airfoil) an increased TE taper of 15 deg was obtained.

The 1.9-m span plate model (20-mm thick, with profiled leading and trailing edges) was vertically mounted in the AWB test section. The respective setup is described in more detail in Ref. [6]. Maximum chord-based *Re* numbers were comparable to full-scale conditions (e.g. corresponding to an aircraft slat at a typical approach speed of u_∞ = 70–90 m/s). The baseline solid TE was realized with a constant 5-deg taper angle and a thickness of h = 0.15 mm.

2.1. Trailing-Edge Modifications

Both models had exchangeable TE sections for tests on a variety of midspan comb-type edge-modifications. Two principally different modifications of the aforementioned solid baseline TEs were tested; (i) TE extensions, and (ii) a slit TE (Figs. 1 and 2).

The 500-mm span "TE extensions" were composed of one single row of cylindrical fibres or needles, respectively. The latter were clamped within a 0.5-mm thin mounting gap in the backplane of specifically designed TE sections which provided the same contour as the thin baseline configurations, but cut-off to gain enough mounting space. Thus, the solid TE thickness at the comb root was h = 1 mm, resulting in geometric steps of 0.25–0.35 mm, depending on the fibre thickness (Fig. 2). These modifications caused a slightly varying chord length compared to the baseline configuration. Comb design parameters which were investigated in the current study included fibre material (flexible polypropylene (PP) fibres vs. stiff steel needles), fibre length (l = 5–100 mm), fibre spacing (slit width between the fibres: s < 0.1 mm to s = 0.3 mm), fibre diameter (h_f = 0.3–0.5 mm), and fibre yawing angle (0 deg vs. 10 deg).

Which is referred to as "slit TE" means a modification at the NACA0012-like airfoil, that preserved the original solid airfoil's geometry and chord length, but containing a slotted midspan TE-region over 400 mm of the span. The slits in this area were realized with a length of l = 45 mm, a width of s = 0.1 mm, and a separation distance (corresponding to the fibre diameter of the TE extensions) of 0.4 mm.

Due to limitations in the manufacturing accuracy of the comb devices the slit width is indicated in mean values.

2.2. Flow Conditions

Flow parameters included *Re* number by varying both flow velocity (u_∞ = 40–60 m/s) and model chord length. Exact alignment of the model airfoils was ensured by differential static pressure measurements. The (flat) plate model was exposed to the flow at a 0-deg angle-of-attack. At the NACA0012-like airfoil, also the effectiveness of TE combs at changing angles-of-attack was tested, which is of interest with regard to a prospective application of comb devices at deployed high-lift flaps. Aerodynamic angle-of-attack α^* was ranging from 0–8.7 deg, corresponding to geometric angles-of-attack of α = 0–14 deg.

From early TE noise studies it is known that the turbulent boundary-layer (TBL) development has a strong influence on the TE noise spectral shape [11, 13]. Therefore, to provide reproducible flow conditions, the boundary layers were symmetrically tripped. For the flat-plate measurements transition was enforced by a 0.1-mm backward-facing step in the contour being located 55 mm downstream of the leading edge. In the case of the NACA0012-like airfoil, a 0.4-mm thick zigzag trip strip (of 12 mm in length, 60-deg serration tip angle) was used with its leading edge being positioned at 9.25 % of the chord length. The effectiveness of the tripping devices and, thus, the actual transition position were verified by infrared thermography and stethoscope measurements. Inflow turbulence levels were in the order of Tu_x = 0.4 %.

Within the current experiments the boundary-layer properties were changed by multiple parameters, i.e. the flow velocity, chord length, profile geometry (in particular TE taper), and the tripping devices. Therefore, additional hot-wire and unsteady surface pressure transducer measurements were conducted at the baseline flat plate configurations to determine steady and unsteady boundary-layer characteristics (such as boundary-layer velocity profiles and the respective integral scales, turbulence intensity, and the spectra of fluctuating velocities or surface pressures, respectively). The hot-wire instrumentation included a fully integrated constant temperature anemometer with built-in signal conditioning and a thermocouple circuit for fluid temperature acquisition and automatic temperature correction. Both single- and cross-wire probes were applied. Measurements of the unsteady surface pressures were realized by 9 flush-mounted miniature sensors (Kulite, type LQ-3H-062-15A with a centred 0.5-mm diameter pinhole), which were placed in an L-shaped array of 4 streamwise positions (at midspan) and 6 spanwise positions in negative z-direction (being located 16 mm upstream of the TE). Analysis was restricted to a frequency range of interest of 0.3–10 kHz, and provided a frequency resolution of 24.4 Hz. The procedure (and most of the major findings) were comparable to the well documented survey in Ref. [11] and will not be repeated here. Within a co-operative work with DLR and LaVision Göttingen, also high-speed particle-image-velocimetry (HS-PIV) measurements [14] were conducted (at the 2-m flat-plate model with a thicker 1-mm TE only). Due to the limited scope of the paper the discussion will mainly refer to the measured boundary-layer displacement thickness δ^* which is the commonly chosen flow parameter in TE noise studies. For comparison, and to provide corresponding boundary-layer information also for the NACA0012-like airfoil, numerical simulations by means of the panel method XFOIL [15] were performed.

2.3. Acoustic Data Acquisition and Processing

A directional microphone system (composed of a reflector and a microphone) was used to extract TE noise from extraneous noise sources. A minimum resolution width of one acoustic wavelength was realized by an ellipsoidal reflector

geometry with a fixed foci separation distance (source-to-microphone distance) of R = 1.15 m, and a reflector diameter of D = 1.4 m, which was designed by Dobrzynski et al. [16]. The measurement principle is based on an optical analogy, using the elliptic mirror surface to create in its near focus an enhanced image of the sound originating from a distinct volume element of the source distribution in its far focus, mirror and microphone being both located in the acoustic farfield [17, 18]. As a consequence of the high-resolution design a system aperture of 63 deg was obtained. In the present study a 1/4-inch B&K condenser microphone (type 4136) without protective grid, to improve omnidirectionality, was employed. For localization of the TE noise sources the system was moved on a traversing cart, providing maps of the noise source strengths on the airfoil surface. For all measurements the directional microphone axis was oriented at 90 deg to the wind tunnel centreline (x-direction). The particular acoustic mirror setups for the respective vertical and horizontal model arrangements and the corresponding measurement coordinate system are shown in Fig. 3. Note the different configuration-dependent TE positions (1–4) in x-direction. For all measurement arrangements the far focus local (source) origin was fixed at the midspan position of the respective (convection corrected) TE locations. Data acquisition provided a measurement accuracy of ± 0.8 dB. A 256-Hz high-pass filter served to suppress low-frequency extraneous noise contributions.

The usage of source localization techniques, such as elliptical or spherical mirror systems in the farfield to determine source location has both advantages and serious drawbacks. One advantage lies in the necessary increase of the signal-to-noise ratio S/N for detection of low-noise sources like TE noise or, as in the current study, the sound emission of highly effective noise reduction means, which are otherwise masked by extraneous tunnel noise contributions. The drawbacks are related to the correct interpretation of the obtained source maps, since the measured distributions of sound source intensities include the effects of the frequency-dependent response function (specific gain and resolution) of the acoustic mirror system, and of characteristics of the actual source distribution. Furthermore, the mirror gain and resolution are severely affected by the free-jet wind-tunnel shear-layer, which itself depends on the respective measurement position and the flow speed [13, 16–18].

Therefore, extensive corrections of the directional microphone data were performed in the current study, to provide absolute source levels and corrected spectral shapes. A comprehensive data reduction procedure to recover the true acoustic source strength must account for (i) extraneous wind-tunnel noise sources, (ii) sound wave convection, (iii) spatial resolution of the reflector, (iv) gain of the system, and (v) noise refraction and scattering while propagating through the open-jet shear-layer. To account for extraneous noise sources, the empty wind-tunnel background noise floor was measured, and background noise corrections were performed for $S/N \geq 3$ dB. The apparent shift in source position due to sound wave convection effects [18] was calibrated and subtracted from the measured x-position. The applied correction for the frequency response of the directional microphone system was mainly based on an early work of Schlinker [13], where TE noise was modelled by simply a two-dimensional line source (distribution of uncorrelated point sources) along the TE. The corrected mean-square farfield sound pressure $\langle p^2 \rangle$, as radiated from the TE, was derived from the measured mean-square farfield sound pressure $\langle p^2_M \rangle$ according to Eqs. 1 (corresponding to Eq. 21 in Ref. [13]):

$$\left\langle p^2 \right\rangle = \frac{\left\langle p_M^2 \right\rangle}{G} \frac{S}{\int_{-S/2}^{+S/2} H(\eta) dy,z} \qquad \text{with} \quad H(\eta) = \left[\frac{2J_1(\eta)}{\eta} \right]^2, \qquad (1)$$

$$\text{and} \qquad \eta = \frac{\pi \, D \, f \, y,z}{c \, R}$$

Herein, the resolution correction, based on Fraunhofer diffraction theory, is represented by the ratio of the span S to the integrated Fraunhofer diffraction pattern $H(\eta)$, with η being the respective diffraction parameter, $J_1(\eta)$ the Bessel function, f the frequency, and c the speed of sound. The subsequent discussion of the results will restrict on a one-third octave band presentation. Therefore, the narrowband formulation of the resolution correction has been used to approximate the one-third octave band characteristics. The applied corrections are displayed in Fig. 3b. Gain G data was available from calibration measurements with a constant power monopole-type calibration "point" source [16]. Detailed information concerning the calibration procedure and the determined system response for a typical measurement position (corresponding to TE position 1, Fig. 3) are provided in Ref. [16]. From these results it is known that shear-layer related effects, i.e. the diminishing and broadening of the measured diffraction patterns, grow important for one-third octave band centre frequencies $f_m > 10$ kHz, so that the applied correction procedure is considered reliable for at least $f_m \leq 10$ kHz. However, in the case of the flat-plate experimental arrangement (with varying chord length) the sound waves propagating to the mirror have to cross a successively growing shear-layer (TE positions 2-4, Fig. 3). From comparative TE noise measurements on the shorter plate configurations at different x-positions a straightforward shear-layer correction (accounting for the total frequency-dependent level fall-off due to the downstream shift of the TE measurement position, when compared to position 1) was evaluated. This simplified correction is presented in Fig. 3c. It was found that for the positions 2-4, shear-layer scattering already becomes relevant for $f_m \geq 4$ kHz, and its effect increases with frequency (leading to a maximum level drop of 3 dB for TE position 4 at $f_m = 20$ kHz). This is due to the increased ratio of turbulence scales in the shear layer when compared to the acoustic wavelength. On this basis the equivalent sound emission corresponding to TE-position 1 could be calculated for a direct comparison of all plate configurations. Due to the frequency dependence of system resolution the lower frequency range was limited to frequen-

cies $f_m \geq 1$ kHz, i.e. data presentation will restrict to 1 kHz $\leq f_m \leq$ 10 kHz.

3. EXPERIMENTAL RESULTS

The evaluation of different noise reduction techniques requires a detailed knowledge of the generation mechanism at the chosen solid reference TE configurations. Therefore, the sound emission and respective TE noise scaling laws have to be determined for these baseline configurations prior to the discussion of the obtained noise reduction results. Fig. 4a shows the normalized TE farfield noise one-third octave band spectra as measured for the different test airfoils in comparison with prediction results ($\alpha = 0$ deg; absolute levels referred to $S = 0.8$ m, $R = 1.15$ m, observer angle $\theta = 90$ deg). Data presentation applies the generally accepted scaling of TBL-TE noise spectra according to a u_∞^5-law, which was originally derived by Ffowcs Williams and Hall [2] for the idealized (non-compact) case of a semi-infinite plate of zero thickness. As has become general practise, a sound pressure amplitude and frequency scaling based on δ^* as "characteristic" length scale has been applied to provide comparison with other existing TE noise data. Where available (flat plate configurations) the measured values of δ^* were used for scaling purposes instead of the XFOIL results. Both are listed in Table 1 *(left)*. The noise prediction was derived from NAFNoise-calculations (which stands for NREL AirFoil Noise [19]) on a 0.4-m chord NACA0012 airfoil at equal test conditions. The underlying calculation is based on integrated XFOIL boundary-layer calculations and an empirical description of TBL-TE noise by Brooks, Pope and Marcolini [10], being derived from extensive NACA0012 measurement results (applying mainly δ^* as scaling parameter, and NACA0012-specific empirical relationships). As shown in Fig. 4a substantial agreement between measurement and prediction results was obtained in terms of the TBL-TE noise peak frequency and the spectral decay beyond its peak, however, an offset of about 3 dB in absolute level is present which may be attributed to different test conditions, and errors in measurement and data reduction procedures. Note that the data in Ref. [10] was taken from coherent output power measurements with their specific advantages and disadvantages, when comparing it with the corrected directional microphone data.

The direct comparison of normalized NACA0012 and flat-plate TE noise spectra shows significant differences in spectral shape which demonstrates that the chosen scaling method does not provide a complete parametric description of the TE noise phenomenon. Note in that context that the 0.8-m plate and the NACA0012-like airfoil in the current test provide approximately the same δ^* (Table 1). From a number of studies it is known that a scaling merely based on δ^* generally does not provide a perfect collapse of normalized spectra; however, its application has more pragmatic reasons concerning the availability of measurement data. In future approaches it may be necessary to suggest other measurable source quantities that might be used instead (or additionally) to achieve the best possible collapse of measured TE noise data to improve both modelling and prediction capability. The scaling of far-field intensity with a typical flow velocity as $(velocity)^5$ and the cardioid-type directivity are fundamental TE noise characteristics which are not affected by unsteady flow properties. However, the spectral peak frequency and spectral shape (particularly the spectral decay beyond its peak) are determined by the incident turbulence which approaches the TE. According to current knowledge - and supported by the shown measurement results - the high-frequency decay law of TE noise beyond its maximum is not universal, but highly dependent on geometry [3, 8, 10].

In the current study it was found that classical TBL-TE noise can not be seen independent from vortex-shedding noise which also contributes to spectral shape differences with respect to the theoretically "sharp" TE (which in fact does not exist in real applications). In Fig. 4a the expected spectral peak for the flat-plate TE noise is not located at the same Strouhal number $St = f\delta^*/u_\infty \approx 0.06$ as for the NACA0012 and has to be presumed in the lower frequency range $f_m \approx 1$ kHz, or $f_m < 1$ kHz which is below the application limit of the directional microphone system. This lacking information was gained from the unsteady surface pressure measurements at the flat-plate configurations, assuming similar spectral patterns (same "characteristic" frequencies) corresponding to the spectral peaks of both unsteady surface pressures and TBL-TE farfield noise [3, 20].

Fig. 4b shows the scaled surface pressure power spectral densities Φ (PSDs, i.e. the narrowband data being normalized to a 1-Hz bandwidth) as obtained from averaging the PSDs of the 6 spanwise-orientated sensors close to the TE, being based on the free stream dynamic pressure q_∞. The normalized spectral peak frequency for the flat plate configurations (which equals the frequency of the coherence maximum between the spanwise separated sensors) was determined as $0.05 \leq f\delta^*/u_\infty \leq 0.08$, which includes also the measured peak frequencies for the NACA0012-like airfoil. The reported range considers also the uncertainty in measuring δ^*, and includes data scatter caused by taking the XFOIL results instead of the measured values. The obtained peak frequencies are listed in Table 1 *(right)*; for the NACA0012-like airfoil the peak frequencies as measured with the directional microphone are included. These "characteristic" frequencies are suggested to be determined by V/λ_h, with the "hydrodynamic wavelength" λ_h being a correlation scale of the eddy structures containing the major part of turbulent energy and V its convective velocity (which is approximately the local mean velocity at the eddy "centre"). The latter is not easy to determine because of the actual TBL vortex structure being more complex than an idealized circular or ring vortex, and the measured V, as obtained from the slope of the cross-spectral phase-shift between streamwise separated sensors, being dependent on the sensor separation distance. Actually, a complex hierarchy of attached eddies is responsible for mean vorticity and most of the turbulent kinetic energy, the sublayer bursting phenomenon being the main contributor to turbulent energy production within the TBL. Adrian et al. [21] draw a consistent picture of the outer TBL structure according to which packets of multiple hairpin

vortices are created at the wall and grow to span the entire TBL. In fact, the measured peak frequencies (Table 1) correspond to large-scale streamwise vortical structures in the order of the TBL thickness δ_{99} or even larger, as was also verified by the analysis of space-time correlation functions of single-point space correlations of HS-PIV measurement data [14]. From the surface pressure measurements at the flat-plate configurations the ratio V/u_∞ was determined as about 0.6–0.7 within the "characteristic" frequency range. This corresponds for the 2-m plate to $\lambda_h \approx 55$–68 mm which is equivalent to 1.8–$2.3\delta_{99}$, or 10–$12\delta^*$, to give just an example. The respective integral scales were determined as $l_x = V/2\pi f\zeta_x \approx 36$–$57$ mm ≈ 7–$10\delta^*$ in the streamwise direction (ζ_x being the streamwise dissipation constant, as obtained from the decay of coherence between streamwise separated sensors, same procedure as in Ref. [11]) and $l_z = V/2\pi f\zeta_z \approx 12$–$15$ mm ≈ 2–$3\delta^*$ in spanwise direction (ζ_z being the respective spanwise dissipation constant).

3.1. Noise Reduction Potential through Comb-Type Trailing-Edges

As shown in Fig. 5 a significant broadband TE noise reduction (ranging from 2 to 10 dB) can be achieved by comb-type TE-modifications, a result which was already documented in Ref. [6]. The same reference data as in Fig. 4 is represented, but compared to the noise emission of these different test airfoils being equipped with the most successful TE extension within this study (flexible, streamwise oriented PP-fibres, $h_f = 0.4$ mm, $l = 45$ mm, $s < 0.1$ mm). In this case the edge-enhancement of sound was eliminated in such a manner that the remaining noise emission from the TE lies only about 3 dB above the extraneous noise of the wind-tunnel empty test section, which determines the actual limit of the applied measurement technique. In Fig. 5a the same level and frequency scaling was applied as in Fig. 4, whereas in Fig. 5b the data is normalized based on a constant scaling length (here $\delta_0 = 1$ mm chosen). From this presentation it is evident that TE noise spectral scaling for the flexible TE-extension was rather based on a constant scaling length than on δ^*. Therefore, the subsequent discussion of the tested TE-modifications, all of them showing the same behaviour, will apply a spectral scaling based on $\delta_0 = 1$ mm.

As known from measurements on different solid TE thicknesses, blunt TEs contribute strong narrowband vortex-shedding noise, being highly dependent on TE taper. Corresponding results for the $h = 1$ mm case are provided in Ref. [6], showing dominating bluntness noise spectral peaks at $St = f\,h/\,u_\infty \approx 0.1$. As an illustration example the one-third octave band spectrum, as measured for the 2-m plate at $u_\infty = 50$ m/s is added in Figure 5b (note in this case the high-frequency spectral decay which equals that of the NACA0012 configuration). Since $h = 1$ mm corresponds to the step adjacent to the origin of the tested TE extensions (Fig. 2) it can be argued that comb devices are also highly effective in reducing TE bluntness noise which is supposed to exist at nearly every real airfoil. The presentation here will confine to the thin reference TEs ($h = 0.15$ mm), however, Fig. 5b should be kept in mind when actual level differences are to be quantified.

3.2. Effect of Flow Parameters

Effect of Turbulent Boundary-Layer Displacement Thickness: As has been stated above and supported by Fig. 5 the TE noise spectra of the comb-type TE-modifications are nearly unaffected by δ^* (and correspondingly, the model chord length), a result which was reproduced for all of the tested comb-type TE-modifications. This scaling behaviour is in contrast to that of TE noise, as radiated from the different solid reference TE configurations, where δ^* is considered an applicable, even though not perfect scaling parameter for TE noise spectra. According to Fig. 5 it is also evident that the achieved frequency-dependent noise reduction is not significantly altered by δ^*.

Effect of Flow Velocity: From Fig. 5 it is obvious that the aforementioned increase of farfield TE noise intensities according to a u_∞^5-law is also valid for the different models being equipped with the flexible TE-extension. This result is in accordance to the analytical solution of the half-plane TE noise problem by Ffowcs Williams and Hall [2]; therein an unchanged velocity dependence compared to a rigid TE is stated also for a "pressure release" TE (which does dot support any normal stress). In addition, Fig. 6a shows the validity of the velocity scaling law for all different kinds of tested comb-type TE-modifications at the NACA0012-like airfoil, i.e. for both the slit TE and the TE extensions (TE extensions in Fig. 6 with $h_f = 0.4$ mm, $l = 45$ mm). Due to the overall identical velocity scaling of TE noise spectra for reference configuration and noise reduction device, the resulting noise reduction remains independent on flow velocity, when a Strouhal number scaling of frequency is applied (i.e. apart from the frequency shift of TE noise spectra with u_∞).

Effect of Angle-of-Attack: As presented in Fig. 6b the TE extensions (the flexible and stiff ones) show only a minor effect of angle-of-attack on TE noise spectra. Contrary to published results from tests on TE serrations [23], no additional high-frequency excess noise was measured, which is of importance with regard to a possible application of such devices as add-on solutions. However, a growing angle-of-attack appears to diminish the overall noise reduction, because solid TE noise emission significantly decreases in the mid-frequency range. This shown angle-of-attack behaviour of the solid reference TE noise spectra is not in accordance with the outcome of available TE noise predictions and published measurement results, and thus, has to be subject of further investigations. In the relevant literature (e.g. Refs. [10, 22]) an increased low-frequency contribution, being shifted to lower frequencies with increasing angle-of-attack, but an almost invariant higher frequency fall-off portion of the spectra are documented. Note that in the current study also the solid slit TE noise spectrum shows an appreciable decay in the mid-frequency range, however less pro-

nounced than for the reference TE. Qualitatively, the measured TE noise emission for a nonzero angle-of-attack may be interpreted as the result of the two different noise contributions, emanating from the upper and lower TBLs; the low-frequency contributions representing the larger eddy scales within the upper boundary-layer, and the high-frequency contributions those of the smaller eddy scales within the lower boundary-layer. Consequently, the mid-frequency drop-off in level (of > 3 dB) may be explained by an absence of medium-sized vortices on both the pressure and suction-side TBL at the TE. However, this explanation is not satisfying from aerodynamic considerations; a detailed comparison with available test data (including measurements of the TBL wall-pressure fluctuations) and results from current noise prediction approaches will have to be the focus of further studies.

3.3. Effect of Trailing-Edge Design Parameters

From a direct comparison of noise measurements on the flat plate (with varying chord length) and the NACA0012-like airfoil, no significant effect of the chosen model airfoils (and thus, the specific incoming flow conditions) on the effectiveness of comb devices was determined. Figs. 5 and 7a have to be regarded in this context. In both cases identical TE-extensions were tested at the NACA0012-like model as well as at the flat plates (hereof, Fig. 7a displays the effect of less successful TE-modifications). For a given TE-modification applied at different models spectral differences are comparably small (and rather difficult to evaluate, referring to the system-inherent measurement accuracy of ± 0.8 dB). Instead of this, comb-type TE noise emission is mainly influenced by the distinct comb design parameters, which directly might alter turbulence characteristics in the comb area and (which is considered even more important) reduce sound radiation efficiency by affecting the edge-scattering process. This simplifies the comb-design optimization process in the current study and may be of major importance for a future transfer of the gained knowledge to complex geometries and flow conditions of full-scale applications (e.g. a slat TE flow). In fact, all model airfoils (within the test range of *Re* numbers) provided the same ranking of the tested TE modifications, and a flexible TE-extension with $h_f = 0.4$ mm, $l = 45$ mm, and $s < 0.1$ mm (as mentioned before, flexible TE-extension in Figs. 5, 6, and 7b) provided the best results for all tested airfoil configurations. The finding that the TE noise emission of comb-type TE modifications is barely affected by the used test airfoil means that the achievable noise reduction benefit for a given TE-modification (in terms of the level differences between spectra of modified and reference TEs) is rather determined by the solid reference TE noise emission itself (Fig. 5b).

In the following the effects of distinct comb design parameters are listed.

Effect of Comb Material: Figs. 5, 6, and 7 illustrate that flexibility of the fibre material is generally beneficial, but not essential to achieve a noise reduction. In fact, the noise reduction capability of stiff flow-permeable TE-modifications has been proven in the current study.

Effect of Fibre Spacing/ Slit Width: According to Fig. 7b, which displays the achievable noise reduction for the NACA0012-like airfoil, the fibre spacing was identified as crucial design parameter. An almost zero-spacing of the fibres ($s < 0.1$ mm) revealed the maximum effect, whereas an increase of the slit width by only about 0.1 mm (which is in the order of the viscous sublayer thickness) leads to a significantly reduced noise reduction capability. However, a more detailed specification (in terms of finer increments within the range of 0 mm < s < 0.1 mm) can not be provided due to the limited manufacturing accuracy. Concerning the noise reduction capacity of the solid slit TE a further improvement can be expected by slit width adjustment.

Effect of Fibre Thickness and Comb Length: The influences of fibre length and fibre diameter (of flexible TE-extensions) were already discussed in Ref. [6]. From this first study it was already known that thicker fibre diameters ($h_f = 0.4$ mm or $h_f = 0.5$ mm) were favourable compared to thin ones ($h_f = 0.3$ mm), and that the specific optimum device length ranges between 30 mm and 60 mm which compares to the measured lengths of streamwise integral turbulence scales l_x within the TBL approaching the TE. As a result of the present study (which comprised tests on TE extensions being successively cut in 5-mm increments) it was found that for the flexible configurations ($s < 0.1$ mm) a minimum fibre length of $l = 30$ mm is necessary for a maximum noise reduction. A further extension of the devices (within the test range of up to $l = 100$ mm) neither increases nor reduces the achieved effect.

Appropriate results were obtained for the stiff slit TE configuration ($s = 0.1$ mm). Here, different comb lengths were realized by blocking the flow-permeable area by spanwise-oriented tape strips. The result also supports a minimum required device length of about 30 mm.

(Yaw-) Fibre Orientation: As measured at both flexible and stiff comb-type TE-extensions ($s \leq 0.1$ mm) at the flat-plate experimental arrangement, fibre orientation in the streamwise direction provided the best noise reduction results. A fibre slant angle of 10 deg resulted in a broadband TE noise increase of about 2 dB.

4. CONCLUSIONS AND FUTURE WORK

The aeroacoustic properties of comb-type trailing-edge modifications on two selected test airfoils were investigated within a set of parametric experiments. An achieved broadband noise reduction of 2–10 dB indicates that the tested devices have the potential to induce changes to the edge discontinuity which is otherwise the cause of strong turbulent boundary-layer edge-scattering noise. It was found that comb devices are highly effective not only in the wide frequency range of turbulent boundary-layer trailing-edge noise (with measured peak frequencies of $0.05 \leq f_m \delta^* / u_\infty \leq 0.08$), but they also eliminate high-amplitude narrowband vortex-shedding noise contributions due to trailing-edge bluntness.

The theoretical modelling of trailing-edge noise, and thus, the accurate prediction of the achieved noise reduction by different edge-geometries is up to now an unsolved problem due to uncertainty over the appropriate flow condition applicable to the edge. The question how viscous effects (realized by the imposition of the Kutta condition) have to be included in theory is relevant for the noise prediction for any type of (solid or flow-permeable) trailing-edge geometry. Actual uncertainties in predicted absolute farfield noise levels are substantially brought about by unspecified edge conditions which can amount level differences of 10 dB or more [3]. In the current study the measured trailing-edge noise spectra were not universal for varying trailing-edge geometries, and the noise reduction potential through comb-type modifications was far more affected by slight modifications of the comb design than by incident flow parameters, e.g. δ^* or u_∞. Accordingly, over the test range of *Re* numbers (2.1 Mio to 7.9 Mio) the obtained ranking of different comb-type trailing-edge extensions, installed on different test airfoils, was independent of both *Re* number and the airfoil geometry (e.g. the trailing-edge taper and chord length). Howe [3] shows that despite of changes in numerical value other typical trailing-edge noise characteristics, such as the $(velocity)^5$-scaling of farfield sound intensity, remain unaffected by implication of the Kutta condition. This statement is perfectly supported by the obtained experimental results, because all of the tested edge-modifications show the same u_∞^5-scaling of trailing-edge noise spectra as the solid reference configurations. It is important to note that this also holds for the tested flexible comb-type devices, being in line with the theoretical findings of Ffowcs Williams and Hall [2] for the case of a limp "pressure release" trailing-edge. As a result of the unchanged velocity scaling behaviour of trailing-edge noise levels the achieved noise reduction by a specific edge-modification remains constant, irrespective of the flow velocity.

In order to attain knowledge of the effective noise reduction mechanisms and scaling laws (and how the edge condition might be adapted) the trailing-edge noise emission was measured in dependence on comb design-parameters, mean flow velocity, boundary-layer characteristics, and angle-of-attack. Within the range of parameters tested so far, an optimized edge-modification has to meet the following requirements: (i) exceeded minimum fibre length, (ii) small fibre spacing, (iii) fibre (yaw-) orientation in flow direction, and (iv) flexible fibre material.

With regard to the significance of different comb design characteristics, it was found that flexibility of the comb material is beneficial but not imperative to achieve a noise reduction. Instead of the material properties, the width and length of the comb slits were identified as crucial design parameters. An almost-zero slit width (< 0.1 mm, comparable to the viscous sublayer thickness) turned out most effective, which leads to the assumption that hydrodynamic absorption in the comb area may be of importance for the noise cancellation process. The required minimum fibre length to achieve maximum noise reduction results was quantified to l = 30 mm, which is in the order of δ_{99} to $2\delta_{99}$. The best match of normalized trailing-edge noise spectra applying the u_∞^5-law for a given comb-type modification was obtained for a Strouhal number and level scaling, based on a constant correlation length. This supports that the noise emission of comb-type trailing-edges is dominated by geometric properties rather than being determined by turbulence scales within the incident boundary-layer flow. In contrast, for solid trailing-edges the effect of the incident turbulence scales on trailing-edge noise emission is well-documented in literature, and scaling of the solid reference trailing-edge noise spectra based on δ^* leads to fairly acceptable results. An important advantage in terms of applicability is that selected flow-permeable edge-extensions show nearly no effect of angle-of-attack on trailing-edge noise spectra. This is in contrast to the effect of trailing-edge serrations [3, 23], which are known to contribute high-frequency excess noise diminishing the overall noise reduction.

The gained knowledge shall be later used for advanced noise reduction concepts which are relevant for a great number of aeronautical, automotive, and naval applications; trailing-edge noise exists at almost any kind of airfoil or flow-immersed surface, e.g. on aircraft components, cooling fans, turbomachinery or wind turbine blades, just to name a few.

Probable applications to be realized in the near future are seen in retrofit solutions for wind-turbine blades, and low *Re* number fans. The development of add-on solutions for current high-lift systems of civil aircraft, e.g. the slat trailing-edge, remains challenging and is considered costly referring to the stringent aeronautic security standards. Technical problems to be solved are employment and stowing kinematics of such comb devices, maintenance (dirt susceptibility, wear-out failure, and icing) as well as the manufacturing. In addition to available computational results [9] the effect of such devices on the aerodynamic performance will have to be quantified in future measurements.

ACKNOWLEDGEMENT

The current work was conducted in the framework of the DLR project "Quiet Air Traffic". The author would like to thank her colleagues from the Technical Acoustics Branch of DLR Braunschweig for their valuable support and helpful discussions throughout the study.

REFERENCES

[1] Argüelles, P., Bischoff, M., Busquin, P., Droste, B. A. C., Evans, R., Kröll, W., Lagardère, J.-L., Lina, A., Lumsden, J., Ranque, D., Rasmussen, S., Reutlinger, P., Robins, R., Terho, H., and Wittlöv, A., "European Aeronautics: A Vision for 2020, Meeting Society's Needs and Winning Global Leadership," KI-34-01-827-EN-C, Rept. of the Group of Personalities, Advisory Council for Aeronautics Research in Europe, Office for Official Publications of the European Communities, Luxembourg, Jan. 2001

[2] Ffowcs Williams, J. E., Hall, L. H., "Aerodynamic Sound Generation by Turbulent Flow in the Vicinity of a Scat-

tering Half-Plane," *Journal of Fluid Mechanics*, Vol. 40, No. 4, 1970, pp. 657-670
[3] Howe, M. S., "Acoustics of Fluid-Structure Interactions," Cambridge University Press, 2000
[4] Blake, W. K., "Mechanics of Flow-Induced Sound and Vibration, Complex Flow-Structure Interactions," *Applied Mathematics and Mechanics*, Vol. 17-II, Academic Press, Inc., Orlando, FL, 1986, pp. 756-767
[5] Mau, K., and Dobrzynski, W., European Patent; "Anordnung zur Minderung des aerodynamischen Lärms an einem Vorflügel eines Verkehrsflugzeuges," No. EP-1314642 B1, filed 2005
[6] Herr, M., and Dobrzynski, W., "Experimental Investigations in Low-Noise Trailing-Edge Design," *AIAA Journal*, Vol. 43, No. 6, 2005, pp. 1167-1175
[7] Lilley, G. M., "A Study of the Silent Flight of the Owl," AIAA Paper 98-2340, 1998
[8] Lilley, G. M., "The Prediction of Airframe Noise and Comparison with Experiment," *Journal of Sound and Vibration*, Vol. 239, No. 4, 2001, pp. 849-859
[9] Ortmann, J., and Wild, J., "Effect of Acoustic Slat Modifications on Aerodynamic Properties of High-Lift Systems," *Journal of Aircraft*, Vol. 44, No.4, 2007, pp. 1258-1263
[10] Brooks, T. F., Pope, D. S., and Marcolini, M. A., "Airfoil Self-Noise and Prediction," NASA Reference Publication 1218, 1989
[11] Brooks, T. F., and Hodgson, T. H., "Trailing Edge Noise Prediction from Measured Surface Pressures," *Journal of Sound and Vibration*, Vol. 78, No. 1, 1981, pp. 69-117
[12] Garcia Sagrado, A., Hynes, T., and Hodson, H., "Experimental Investigation into Trailing Edge Noise Sources," AIAA-Paper 2006-2476, May 2006
[13] Schlinker, R. H., "Airfoil Trailing Edge Noise Measurements with a Directional Microphone," AIAA-Paper 77-1269, Oct. 1977
[14] Schröder, A., Dierksheide, U., Wolf, J., Herr, M., Kompenhans, J.: Investigation on Trailing-Edge Noise Sources by means of High-Speed PIV, 12th International Symposium on Application of Laser Techniques to Fluid Mechanics, Lisbon, Portugal, 12–15 July 2004
[15] Drela, M., and Youngren, H., "XFOIL 6.94 User Guide," Massachusetts Institute of Technology, Cambridge, MA, URL: http://web.mit.edu/drela/Public/web/xfoil/, 2001
[16] Dobrzynski, W., Nagakura, K., Gehlhar, B., and Buschbaum, A., "Airframe Noise Studies on Wings with Deployed High-Lift Devices," AIAA-Paper 98-2337, June 1998
[17] Grosche, F.-R., Stiewitt, H., and Binder, B., "Acoustic Wind-Tunnel Measurements with a Highly Directional Microphone," *AIAA Journal*, Vol. 15, No. 11, 1977, pp. 1590-1596
[18] Sen, R., "Interpretation of Acoustic Source Maps made with an Elliptic-Mirror Directional Microphone System," AIAA-Paper 96-1712, May 1996
[19] Moriarty, P., "NAFNoise User's Guide," National Wind Technology Centre, National Renewable Energy Laboratory, Golden, CO, URL: http://wind.nrel.gov/designcodes/simulators/NAFNoise, July 2005
[20] Yu, J. C., and Tam, C. K. W., "Experimental Investigation of the Trailing Edge Noise Mechanism," *AIAA Journal* Vol. 16, No. 10, 1978, pp. 1046-1052
[21] Adrian, R. J., Meinhart, C. D., and Tomkins, C. D., "Vortex Organization in the Outer Region of the Turbulent Boundary Layer," *Journal of Fluid Mechanics*, Vol. 422, 2000, pp. 1-54
[22] Hutcheson, F. V., and Brooks, T. F., "Effects of Angle of Attack and Velocity on Trailing Edge Noise," AIAA-Paper 2004-1031, Jan. 2004
[23] Braun, K. A., Gordner, A., v. d. Borg, N. J. C. M., Dassen, A. G. M., Doorenspleet, F., and Parchen, R., "Serrated Trailing Edge Noise (STENO)," Final Rept. of EU-Project JOR3-CT95-0073, Inst. for Computer Applications, Univ. of Stuttgart, Germany, April 1998

TABLES

Table 1 *(values on the left)*: Measured and calculated δ^* at the TE [XFOIL-results in brackets], mm / *(values on the right)*: Measured TBL-TE noise spectral peak frequency, kHz.

Configuration	Wind speed, m/s		
	40	50	60
2.0-m plate	5.6 [5.4] / 0.4	5.6 [5.2] / 0.6	5.6 [5.1] / 0.6
1.6-m plate	5.0 [4.6] / 0.6	4.9 [4.3] / 0.7	4.8 [4.2] / 0.8
1.2-m plate	3.7 [3.5] / 0.7	3.7 [3.4] / 0.9	3.5 [3.3] / 0.9
0.8-m plate	2.7 [2.6] / 0.8	2.6 [2.5] / 1.1	2.6 [2.4] / 1.2
NACA0012-like airfoil	- [2.5] / 1.1	- [2.3] / 1.3	- [2.3] / 1.5

FIGURES

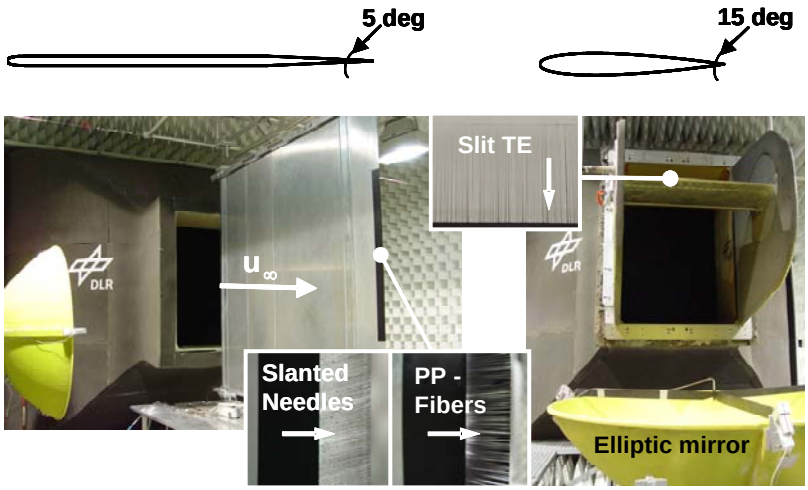

Figure 1 Experimental setups in the AWB test section.

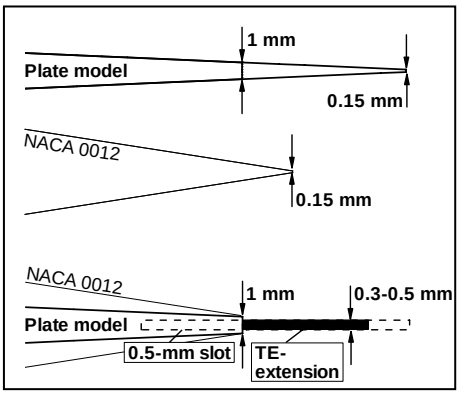

Figure 2 Geometry of TE sections.

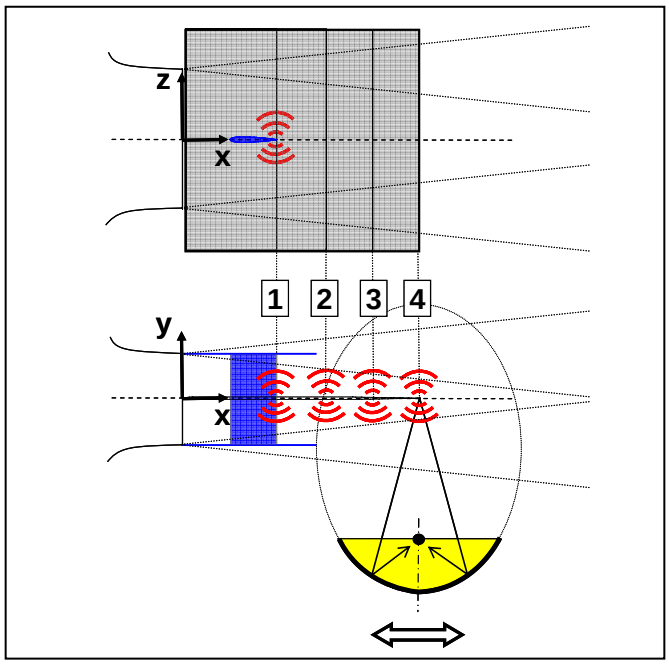

a)

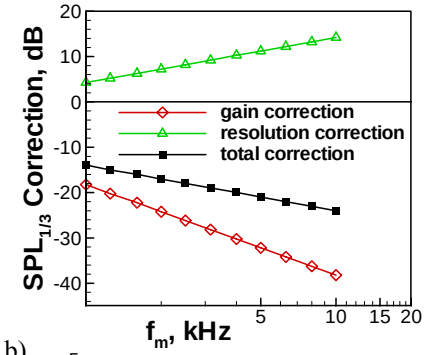

b)

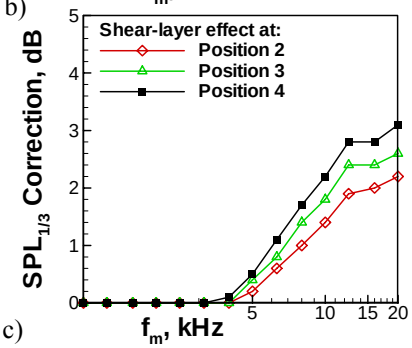

c)

Figure 3 a) Elliptical mirror setup and measurement coordinate system. b) Simplified shear-layer correction. c) One-third octave band sound pressure level correction according to Eqs. 1 (for S = 0.8 m).

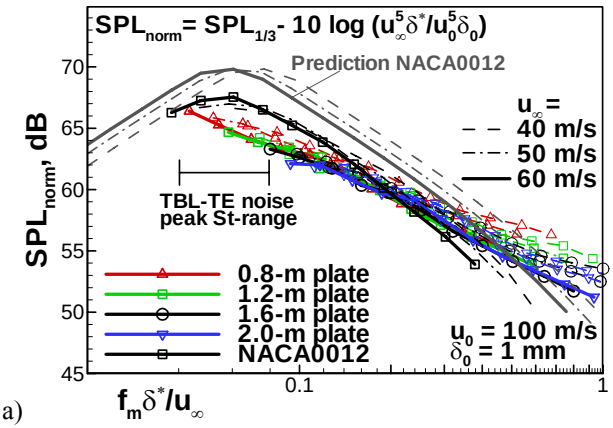

a)

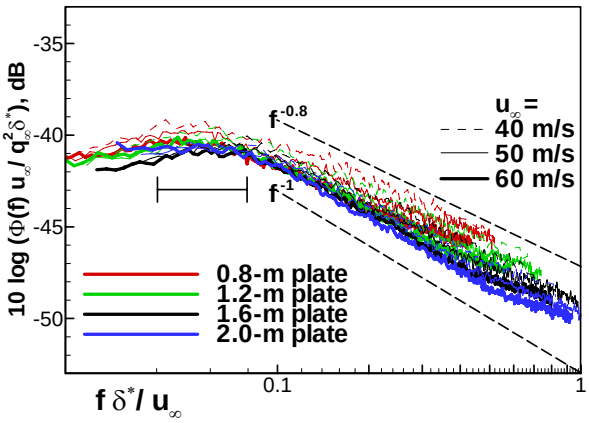

b)

Figure 4 TBL-TE noise spectral peak scaling behaviour for the solid reference TEs (α = 0 deg). a) Normalized TE noise one-third octave band spectra in comparison with prediction results. b) Normalized unsteady surface pressure PSDs.

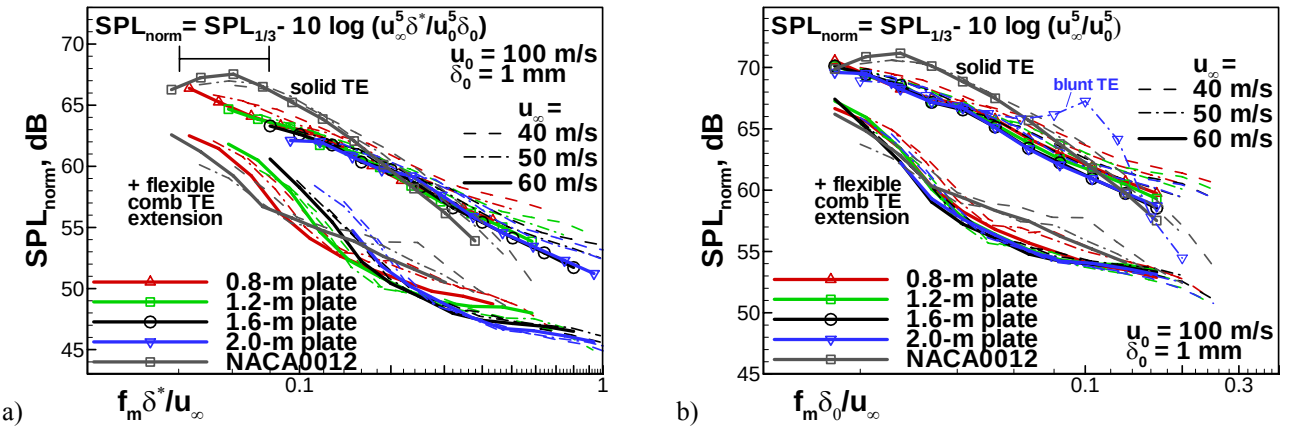

Figure 5 TE Level and frequency scaling behaviour of TE noise one-third octave band spectra, $\alpha = 0$ deg. a) Spectral scaling based on δ^*. b) Spectral scaling based on a constant scaling length δ_0.

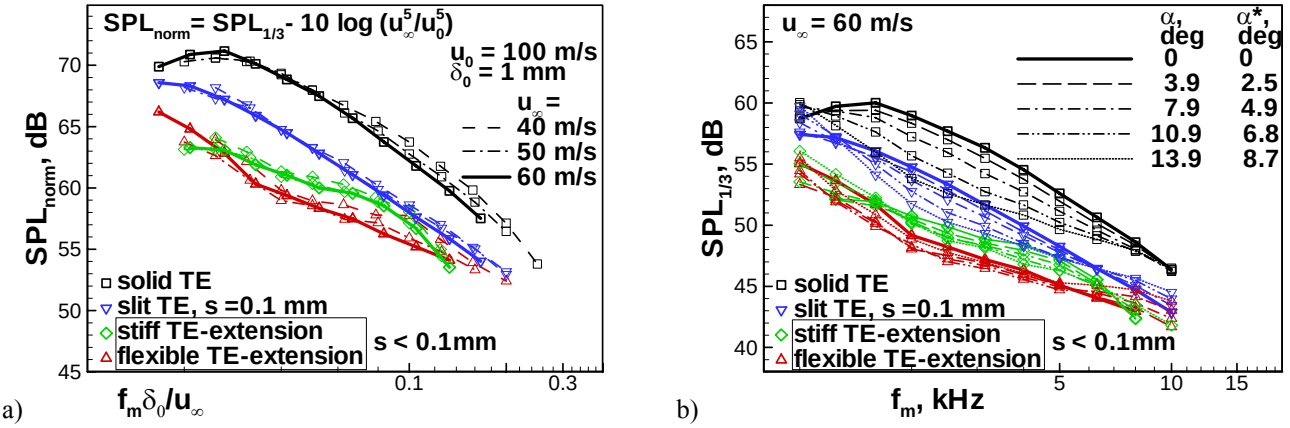

Figure 6 Sound emission of selected TE-modifications at the NACA0012-like airfoil. a) Effect of flow velocity, $\alpha = 0$ deg. b) Effect of varying angle-of-attack.

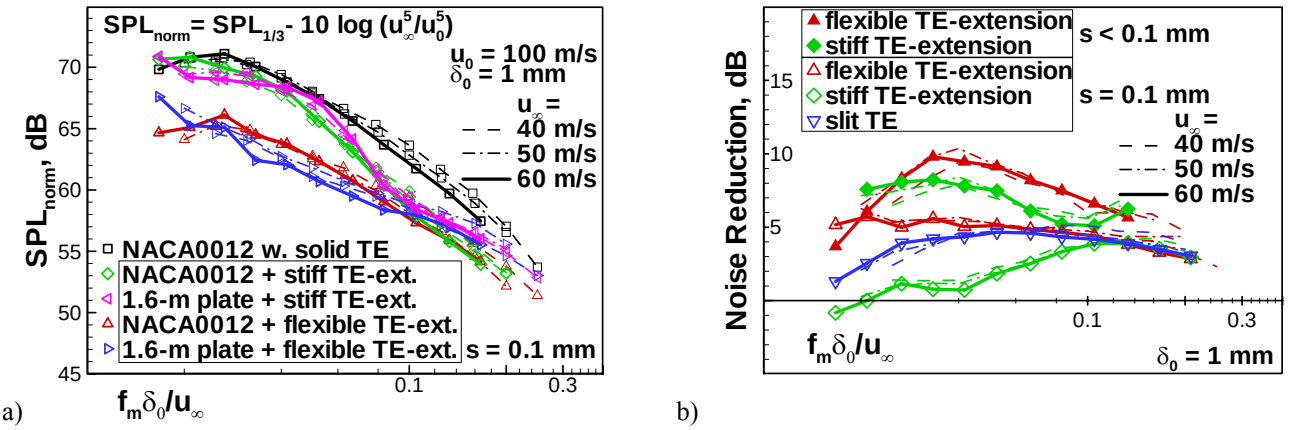

Figure 7 Effect of comb material and fibre spacing on the noise reduction, $\alpha = 0$ deg. a) Varying material of combs at different models, $l = 55$ mm, $h_f = 0.4$ mm. b) Varying slit width of TE modifications at the NACA0012-like airfoil, $l = 45$ mm, $h_f = 0.4$ mm.